Monthly Notices
of the
ROYAL ASTRONOMICAL SOCIETY

MNRAS **430,** 2002–2017 (2013) doi:10.1093/mnras/stt026

Molecular hydrogen and [Fe II] in active galactic nuclei – III. Low-ionization nuclear emission-line region and star-forming galaxies

R. Riffel,[1]★† A. Rodríguez-Ardila,[2] I. Aleman,[1] M. S. Brotherton,[3] M. G. Pastoriza,[1] C. Bonatto[1] and O. L. Dors Jr[4]

[1]*Departamento de Astronomia, Universidade Federal do Rio Grande do Sul, Av. Bento Gonçalves 9500, Porto Alegre, RS, Brazil*
[2]*Laboratório Nacional de Astrofísica/MCTI – Rua dos Estados Unidos 154, Bairro das Nacões, CEP 37504-364, Itajubá, MG, Brazil*
[3]*Department of Physics and Astronomy, University of Wyoming, Laramie, WY 82071, USA*
[4]*Universidade do Vale do Paraíba, Av. Shishima Hifumi 2911, CEP 12244-000, São José dos Campos, SP, Brazil*

Accepted 2013 January 3. Received 2012 December 21; in original form 2012 November 1

ABSTRACT

We study the kinematics and excitation mechanisms of H_2 and [Fe II] lines in a sample of 67 emission-line galaxies with Infrared Telescope Facility SpeX near-infrared (0.8–2.4 μm) spectroscopy together with new photoionization models. H_2 emission lines are systematically narrower than narrow-line region lines, suggesting that the two are, very likely, kinematically disconnected. The new models and emission-line ratios show that the thermal excitation plays an important role not only in active galactic nuclei but also in star-forming galaxies. The importance of the thermal excitation in star-forming galaxies may be associated with the presence of supernova remnants close to the region emitting H_2 lines. This hypothesis is further supported by the similarity between vibrational and rotational temperatures of H_2. We confirm that the diagram involving the line ratios H_2 2.121 μm/Brγ and [Fe II] 1.257 μm/Paβ is an efficient tool for separating emission-line objects according to their dominant types of activities. We suggest new limits to the line ratios in order to discriminate between the different types of nuclear activities.

Key words: line: formation – molecular processes – galaxies: Seyfert – infrared: galaxies.

1 INTRODUCTION

Molecular gas emission has been detected in the inner few tens of parsecs of the central region of emission-line galaxies (e.g. Alloin & Galliano 2002; Gratadour et al. 2003; Riffel, Rodríguez-Ardila & Pastoriza 2006a; Riffel et al. 2006b, 2008a; Storchi-Bergmann et al. 2010; Riffel & Storchi-Bergmann 2011a,b). However, the origin of these lines remains unclear. They appear in objects classified from starburst (SB) to active galactic nucleus (AGN) dominated. In AGNs, unification models predict the presence of a dusty molecular torus that obscures the central source from some viewing angles, thus creating apparently different AGN classes (e.g. Seyfert 1, Sy1, and Seyfert 2, Sy2, galaxies). In order to block the radiation coming from the central source, the torus must have a very large optical depth (tens of magnitudes), thus serving as a natural reservoir of molecular gas. For example, Gratadour et al. (2003, see their fig. 4) propose that the torus is the source of the H_2 emission lines observed in NGC 1068. However, integral field unit (IFU) spectroscopy of this source shows that the molecular gas is distributed along the galaxy and is spatially correlated with a young stellar population (30 Myr old; Storchi-Bergmann et al. 2012).

Observational evidence has confirmed that circumnuclear/nuclear SBs can coexist in objects harbouring AGNs (e.g. Mizutani, Suto & Maihara 1994; Imanishi & Dudley 2000; Contini et al. 2002; Sturm et al. 2002; Rodríguez-Ardila & Viegas 2003; Imanishi & Wada 2004; Storchi-Bergmann et al. 2005; Shi, Gu & Peng 2006). However, in the case of low-luminosity AGNs, no strong SB evidence is found, but significant fractions of intermediate-age stars are detected (Ivanov et al. 2000; Cid Fernandes et al. 2004, 2005, 2010; González Delgado et al. 2004, and references therein). Thus, if star formation is taking place or occurred recently, the presence of molecular clouds associated with the star-forming regions should leave spectral signatures that may contaminate the AGN spectrum. Therefore, whether the H_2 lines observed in AGNs are directly associated with either the molecular dusty torus or the circumnuclear gas remains an open question. Alternatively, the molecular gas may be directly associated with the AGN, but distributed within the circumnuclear region. This later scenario is supported by the fact that the H_2 gas is most probably

★ E-mail: riffel@ufrgs.br
† Visiting Astronomer at the Infrared Telescope Facility, which is operated by the University of Hawaii under Cooperative Agreement no. NCC 5-538 with the National Aeronautics and Space Administration, Office of Space Science, Planetary Astronomy Program.

arranged in a disc surrounding the nucleus (Reunanen, Kotilainen & Prieto 2002, 2003; Neumayer et al. 2007). In this picture, shocks by radio jets and X-ray heating are plausible excitation mechanisms for the H_2 molecule (Knop et al. 1996; Reunanen et al. 2002; Dors et al. 2012).

As shown by Rodríguez-Ardila et al. (2004), Rodríguez-Ardila, Riffel & Pastoriza (2005) and Riffel et al. (2006a) in the study of 51 objects, mostly AGNs, molecular hydrogen is detected in almost all Sy2 and in about 80 per cent of the Sy1 sources. Interestingly, the four SB galaxies in Riffel et al. (2006a) also show the presence of molecular hydrogen emission. However, these previous studies have not included a statistically significant number of low-ionization nuclear emission-line region (LINER) and star-forming galaxies (SFGs). In fact, up to now, only a few investigations have included these types of sources (e.g. Larkin et al. 1998). These classes deserve separate analyses, as it is expected that the active nucleus has very little influence on their emission-line spectrum.

H_2 infrared (IR) emission lines may be produced by the radiative de-excitation following collisional excitation (thermal process) or ultraviolet (UV; 6–18 eV) photon absorption (non-thermal process). H_2 may also be formed in an excited state, after which de-excitation also leads to the emission of IR lines. This mechanism is, however, not very important in a hot or strongly UV/X-ray-irradiated gas (e.g. Aleman & Gruenwald 2011) as AGNs. H_2 IR emission can be significant in regions illuminated by UV photons (Black & van Dishoeck 1987; Sternberg & Dalgarno 1989) or X-rays (Lepp & McCray 1983; Maloney, Hollenbach & Tielens 1996), as well as in shocks (Hollenbach & McKee 1989). In each case, a different emission-line spectrum is expected and, therefore, the relative intensities among the H_2 emission lines may be used to discriminate between the powering mechanisms (e.g. Mouri 1994), keeping in mind that multiple emitting regions and multiple mechanisms may simultaneously be present (Rodríguez-Ardila et al. 2004, 2005; Riffel et al. 2006b, 2008a; Storchi-Bergmann et al. 2009; Riffel & Storchi-Bergmann 2011b).

Rodríguez-Ardila et al. (2004, 2005) carried out a pioneering study of the H_2 excitation mechanisms in a sample of Seyfert galaxies. The innovation of these investigations compared to previous ones (Veilleux, Goodrich & Hill 1997; Larkin et al. 1998; Reunanen et al. 2002, 2003) is that their integrated spectra cover the inner 300 pc in most of the sample, minimizing the host galaxy contamination and maximizing the number of diagnostic lines observed. In addition, [Fe II] and H_2 emission lines are usually suggested to form in the same region, and the evidence accumulated shows that forbidden iron emission in AGNs can have different sources, but very likely, all directly related to the central engine (Forbes & Ward 1993; Goodrich, Veilleux & Hill 1994; Simpson et al. 1996; Alonso-Herrero et al. 1997; Mouri, Kawara & Taniguchi 2000; Rodríguez-Ardila et al. 2004; Davies et al. 2005; Rodríguez-Ardila et al. 2005; Riffel et al. 2006b, 2008a; Storchi-Bergmann et al. 2009; Riffel & Storchi-Bergmann 2011b; Dors et al. 2012, and references therein). Thus, it is interesting to study the excitation mechanisms leading to H_2, together with the processes responsible for the [Fe II] emission lines.

With the above in mind, we present a study of the excitation mechanisms leading to the emission of H_2 and [Fe II] for a sample of nearby LINERs and SFGs. We present 16 new spectra acquired with the same instrumentation employed by Rodríguez-Ardila et al. (2004, 2005) and Riffel et al. (2006a), with simultaneous observations of the *JHK* bands, eliminating differences in aperture and seeing across the bands. The samples combined correspond to a homogeneous data set with ∼70 sources. To date this is the largest number of galaxies used to study the nuclear excitation mechanisms of H_2 and [Fe II].

This paper is structured as follows. Section 2 presents the observations and data reduction steps. Section 3 discusses the kinematics of the H_2 and [Fe II] gas inferred from their line profiles. In Section 4, the excitation mechanisms of the H_2 IR lines in AGN are discussed using new photoionization models for AGNs and SBs. The calculated emission is compared to the observed H_2-line ratios in a 1–0 S(2)/1–0 S(0) versus 2–1 S(1)/1–0 S(1) diagnostic diagram. Section 5 analyses the line ratios H_2 2.121 μm/Brγ and [Fe II] 1.257 μm/Paβ for different emission-line objects and the apparent correlation between these ratios over a large range of values. It also discusses the difference in these ratios for different nuclear activity types. Concluding remarks are given in Section 6. A Hubble constant of 75 km s^{-1} Mpc^{-1} will be used throughout this work in order to be consistent with our previous studies.

2 OBSERVATIONS AND DATA REDUCTION

Near-infrared (NIR) spectra in the range of 0.8–2.4 μm were obtained on 2010 October 4, 6 and 7 with the SpeX spectrometer (Rayner et al. 2003) attached to the NASA 3-m Infrared Telescope Facility (IRTF). The detector is a 1024 × 1024 ALADDIN 3 InSb array with a spatial scale of 0.15 arcsec per pixel. Simultaneous wavelength coverage was obtained by means of prism cross-dispersers. A 0.8 × 15 arcsec^2 slit was used during the observations, giving a spectral resolution of 360 km s^{-1}. Both the arc lamp spectra and the night-sky spectra are consistent with this value. The seeing varied between 0.4 and 0.7 arcsec over the different nights.

Due to the extended nature of the sources, the observations were done by nodding in an object–sky–object pattern with typical individual integration times of 120 s and total on-source integration times between 18 and 58 min. During the observations, A0 V stars were observed near each target to provide telluric standards at similar air masses. They were also used to flux calibrate the sample. Table 1 shows the observation log. The galaxies are listed in order of right ascension, and the number of exposures refers to on-source integrations.

Spectral extraction and wavelength calibration were performed using the SPEXTOOL, software developed and provided by the SpeX team for the IRTF community (Vacca, Cushing & Rayner 2003),[1] following the same procedures as described by Rodríguez-Ardila et al. (2004). Column 10 of Table 1 lists the radius of the integrated region, with the centre at the peak of the continuum light distribution for each object of the sample. No effort was made to extract spectra at positions different from the nuclear region, even though some objects show evidence of extended emission. Telluric absorption correction and flux calibration were applied to the individual one-dimensional spectra by means of the IDL routine XTELLCOR (Vacca et al. 2003).

The one-dimensional wavelength and flux-calibrated spectra were then corrected for redshift, determined from the average z measured from the position of [S III] 0.953 μm, Paδ, He I 1.083 μm, Paβ and Brγ. Final reduced spectra, in the spectral regions of interest in this work, are plotted in Figs 1 and 2.

[1] SPEXTOOL is available from the IRTF web site at http://irtf.ifa.hawaii.edu/Facility/spex/spex.html

Table 1. Observation log and basic properties of the sample.

Source	Activity	Activity reference	Obs. date	Exp. time (s)	Airmass	RA	Dec.	z	Pos. angle (deg)	Radius (pc)
NGC 23	SFG	1	2010 10 07	29 × 120	1.04	$00^h09^m53\overset{s}{.}4$	$+25^d55^m26^s$	0.015 7202	330	609
NGC 520	SFG	2	2010 10 04	16 × 120	1.04	$01^h24^m35\overset{s}{.}1$	$+03^d47^m33^s$	0.008 0367	300	311
NGC 660	LINER/H II	2,3,4	2010 10 06	24 × 120	1.01	$01^h43^m02\overset{s}{.}4$	$+13^d38^m42^s$	0.002 9152	33	107
NGC 1055	LINER/H II	2,3,4	2010 10 04	16 × 120	1.07	$02^h41^m45\overset{s}{.}2$	$+00^d26^m35^s$	0.003 6267	285	210
NGC 1134	SFG	5	2010 10 04	16 × 120	1.11	$02^h53^m41\overset{s}{.}3$	$+13^d00^m51^s$	0.012 9803	0	503
NGC 1204	LINER	6	2010 10 07	16 × 120	1.23	$03^h04^m39\overset{s}{.}9$	$-12^d20^m29^s$	0.015 4058	66	597
NGC 1222	SFG	7	2010 10 06	24 × 120	1.13	$03^h08^m56\overset{s}{.}7$	$-02^d57^m19^s$	0.008 2097	315	270
NGC 1266	LINER	7	2010 10 07	18 × 120	1.09	$03^h16^m00\overset{s}{.}7$	$-02^d25^m38^s$	0.007 7032	0	298
UGC 2982	SFG	8	2010 10 04	9 × 120	1.11	$04^h12^m22\overset{s}{.}4$	$+05^d32^m51^s$	0.017 7955	295	689
NGC 1797	SFG	1	2010 10 07	16 × 120	1.23	$05^h07^m44\overset{s}{.}9$	$-08^d01^m09^s$	0.015 4111	66	597
NGC 6814	Sy1	7	2010 10 07	16 × 120	1.17	$19^h42^m40\overset{s}{.}6$	$-10^d19^m25^s$	0.005 6730	0	220
NGC 6835	?	–	2010 10 06	22 × 120	1.21	$19^h54^m32\overset{s}{.}9$	$-12^d34^m03^s$	0.005 7248	70	166
UGC 12150	LINER/H II	9	2010 10 04	15 × 120	1.08	$22^h41^m12\overset{s}{.}2$	$+34^d14^m57^s$	0.021 4590	37	748
NGC 7465	LINER/Sy 2	10	2010 10 06	12 × 120	1.03	$23^h02^m01\overset{s}{.}0$	$+15^d57^m53^s$	0.006 6328	340	257
NGC 7591	LINER	7	2010 10 07	16 × 120	1.03	$23^h18^m16\overset{s}{.}3$	$+06^d35^m09^s$	0.016 5841	0	642
NGC 7678	SFG	11	2010 10 04	16 × 120	1.01	$23^h28^m27\overset{s}{.}9$	$+22^d25^m16^s$	0.012 0136	90	419

Note. SFG: star-forming galaxies (SB or H II galaxies). LINER/H II were assumed as pure LINERs in the text. References: (1) Balzano (1983); (2) Ho, Filippenko & Sargent (1997a); (3) Ho et al. (1997b); (4) Filho et al. (2004); (5) Condon, Cotton & Broderick (2002); (6) Sturm et al. (2006); (7) Pareira-Santaella et al. (2010); (8) Schmitt et al. (2006); (9) Veilleux et al. (1995); (10) Ferruit, Wilson & Mulchaey (2000); (11) Gonçalves, Veron & Veron-Cetty (1998).

3 ON THE MOLECULAR GAS KINEMATICS

The main goal of this section is to discuss how the velocity width of the H_2 2.1213 μm emission line is compared to that of [Fe II] and [S III] in different objects. This provides important constraints to the location of the molecular gas and allows a comparison between this region with different types of nuclear activities. It is worth mentioning that the nuclear activity used here (Table 1) comes primarily from optical studies and was taken from the NASA/IPAC Extragalactic Database (NED). However, NIR emission-line ratios may reveal the presence of 'hidden' AGNs (see Section 5).

Previous results, mainly on Seyfert galaxies, are controversial. An imaging study of H_2 emission (Quillen et al. 1999) shows that the H_2 gas is distributed on scales of a few hundred parsecs from the nucleus. In addition, the fact that the H_2 emission was found to coincide with [O III] and Hα+[N II] for some sources led the authors to suggest that the molecular gas may follow the narrow-line region (NLR) gas distribution. Schinnerer, Eckart & Tacconi (1999) suggest that the molecular gas in NGC 1068 and NGC 3727 originates from a warped disc with a radius smaller than $\sim$ 75 pc. These latter results are supported by those of Rodríguez-Ardila et al. (2004, 2005), who found that the H_2 2.1213 μm emission is spectroscopically unresolved or with full width at half-maximum (FWHM) systematically narrower than that of the NLR forbidden lines in Seyfert galaxies. This was interpreted in terms of a kinetic disconnection between the molecular and the NLR gas. Further support to this hypothesis comes from IFU studies of AGNs, which suggest that the H_2 is in the galaxy plane, from the centre up to the field limit ($\sim$500 pc), while the ionized gas is observed up to high latitudes (Riffel et al. 2006b, 2008a; Davies et al. 2009; Müller Sánchez et al. 2009; Storchi-Bergmann et al. 2009, 2010; Riffel & Storchi-Bergmann 2011a,b).

In order to study the H_2 and [Fe II] lines in LINERs and SFGs, and to complete our analysis of these transitions in emission-line objects, we have followed the methodology of our previous studies. We assume that the widths of the forbidden lines (or NLR gas in the case of AGNs) reflect the large-scale motions of the emitting clouds in the gravitational potential of the central mass. As a consequence, similar FWHM of molecular and atomic forbidden lines would indicate that these species are co-spatial.[2]

Table 2 lists the intrinsic FWHM of [S III] 0.9531 μm, [Fe II] 1.2567 μm and H_2 1.957, 2.0332, and 2.121 μm. To obtain the intrinsic FWHM, the instrumental width was subtracted from the observed line width in quadrature. The errors in FWHM ($\sim$30 km s^{-1}) are dominated by the uncertainty in the continuum placement. To ensure that the intrinsic FWHM is equal to or larger than the instrumental one (360 km s^{-1}), a line was considered to be spectroscopically resolved if its measured FWHM was larger than 500 km s^{-1}. Thus, lines with FWHM equal to 360 km s^{-1} in Table 2 may have measured values in the range of 360 km s^{-1} $\leq$ FWHM $\leq$ 500 km s^{-1}.

Fig. 3 compares the observed line profiles of [S III] 9531 Å (dotted line), [Fe II] 1.257 μm (dashed line) and H_2 2.122 μm (full line) for a subsample of our sources (those exhibiting all the three lines). Clearly, [S III] and [Fe II] tend to be broader than H_2, following the same trend as observed in Seyfert galaxies (Rodríguez-Ardila et al. 2004, 2005).

To better understand the kinematics of the gas emitting the different lines in the sources of different classification, we show in Fig. 4 a fractional histogram of the FWHM values of the three lines used in Fig. 3 for the data presented in Table 2 plus literature data taken from Rodríguez-Ardila et al. (2004, 2005). This plot shows that the molecular gas follows different kinematics than that followed by the atomic forbidden emission-line gas not only in Seyferts, but also in LINERs and SFGs. The previous work supports this disconnection in Seyfert galaxies and suggests that the gas is arranged in a disc surrounding the nuclear region (Reunanen et al. 2002, 2003). Further support for this hypothesis comes from Gemini-IFU studies (Riffel et al. 2006b, 2008a; Storchi-Bergmann et al. 2009, 2010; Riffel & Storchi-Bergmann 2011a,b), which suggest that the H_2 is located

[2] It is worth mentioning that only because two lines have similar FWHMs they are not proved to be co-spatial. For instance, they could originate approximately in the same region but from different gas layers with different physical conditions. Even when lines originate from exactly the same gas, different line profiles (or FWHM) may result from radiative transfer effects.

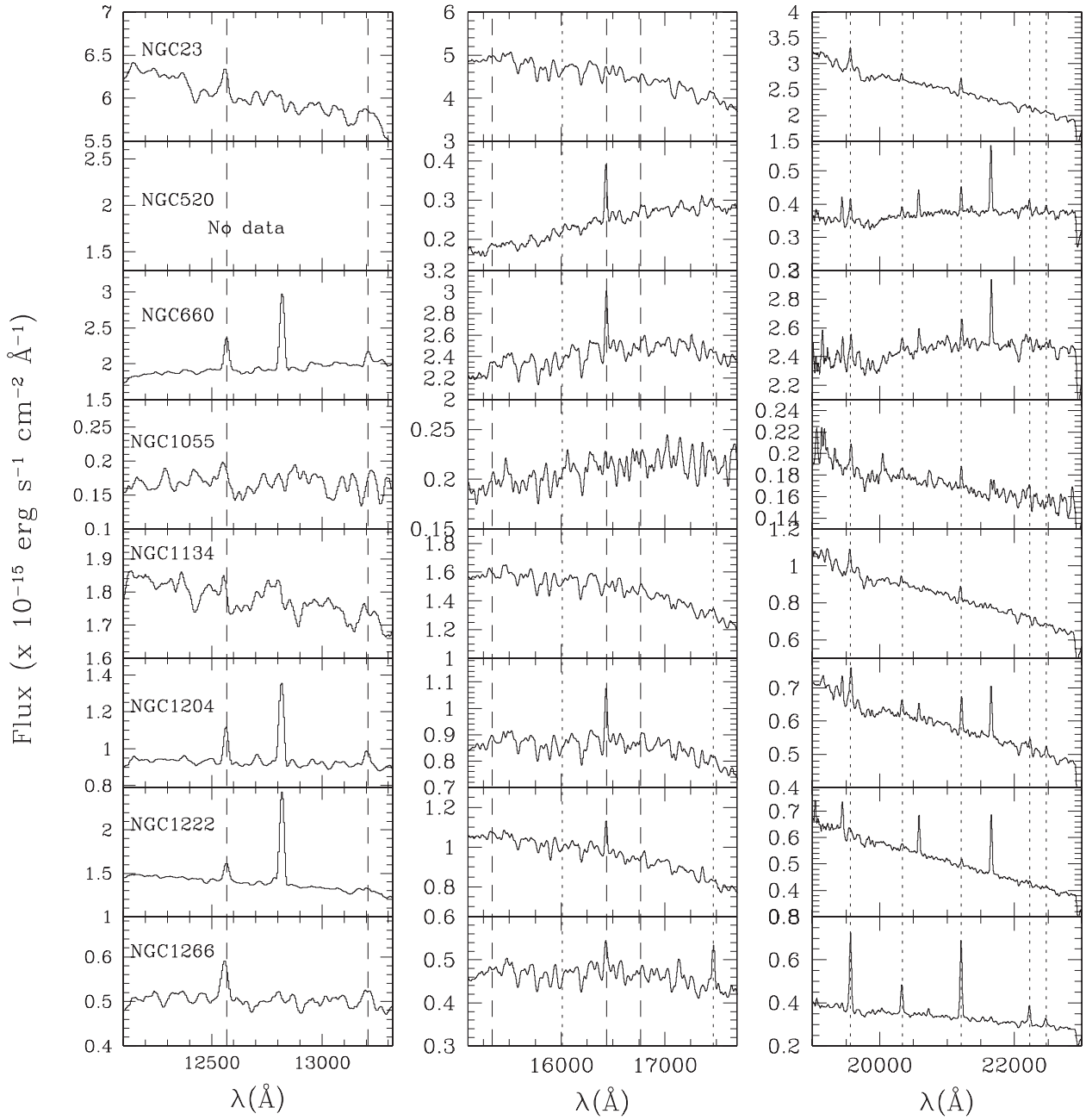

Figure 1. SpeX final reduced spectra, in the Earth's frame of reference, centred near Paβ (left-hand panel), the *H* band (1.60 μm, middle panel) and Brγ (right-hand panel). The observed flux is in units of 10^{-15} erg cm^{-2} s^{-1} Å^{-1}. The identified [Fe II] (dashed lines) and H_2 lines (dotted lines) are marked in the spectra.

in the galaxy plane and is distributed along the whole field, while the ionized gas is observed up to high latitudes from the galaxy plane.

In summary, the observational evidence presented here confirms that H_2 is common within the inner few hundred parsecs of emission-line galaxies, regardless of type. The molecular gas follows different kinematics than that of the ionized gas, suggesting that the two emissions are not co-spatial. The H_2 lines are narrower than the forbidden ones, in particular [S III]. A possible explanation involves atomic gas outflow. Indeed, Riffel et al. (2013) have shown very recently that the velocity dispersion of gas restricted to the plane (H_2 gas) does not correlate with that of bulge stars. On the other hand, the velocity dispersion of gas extending to higher latitudes (such as the [Fe II] emitting gas) is similar to that of the galaxy bulge stars. Higher velocity dispersions of [Fe II] relative to stars are probably due to an extra heating provided by a nuclear AGN outflow. In such a scenario, the atomic gas could be farther out from the supermasive black hole (SMBH) than the molecular gas. Another possibility worth mentioning is the atomic gas being closer to the SMBH than the molecular gas and, thus, being more affected by the gravitational pull of the putative SMBH in AGNs. Such a possibility is related to the fact that [S III] is a higher ionization line and, thus, its bulk should be formed more inwards in the NLR than [Fe II] and H_2. Thus, the unresolved FWHM of H_2 in almost all objects implies that the molecular gas is probably not gravitationally bound to the SMBH, but to the collective gravitational potential of

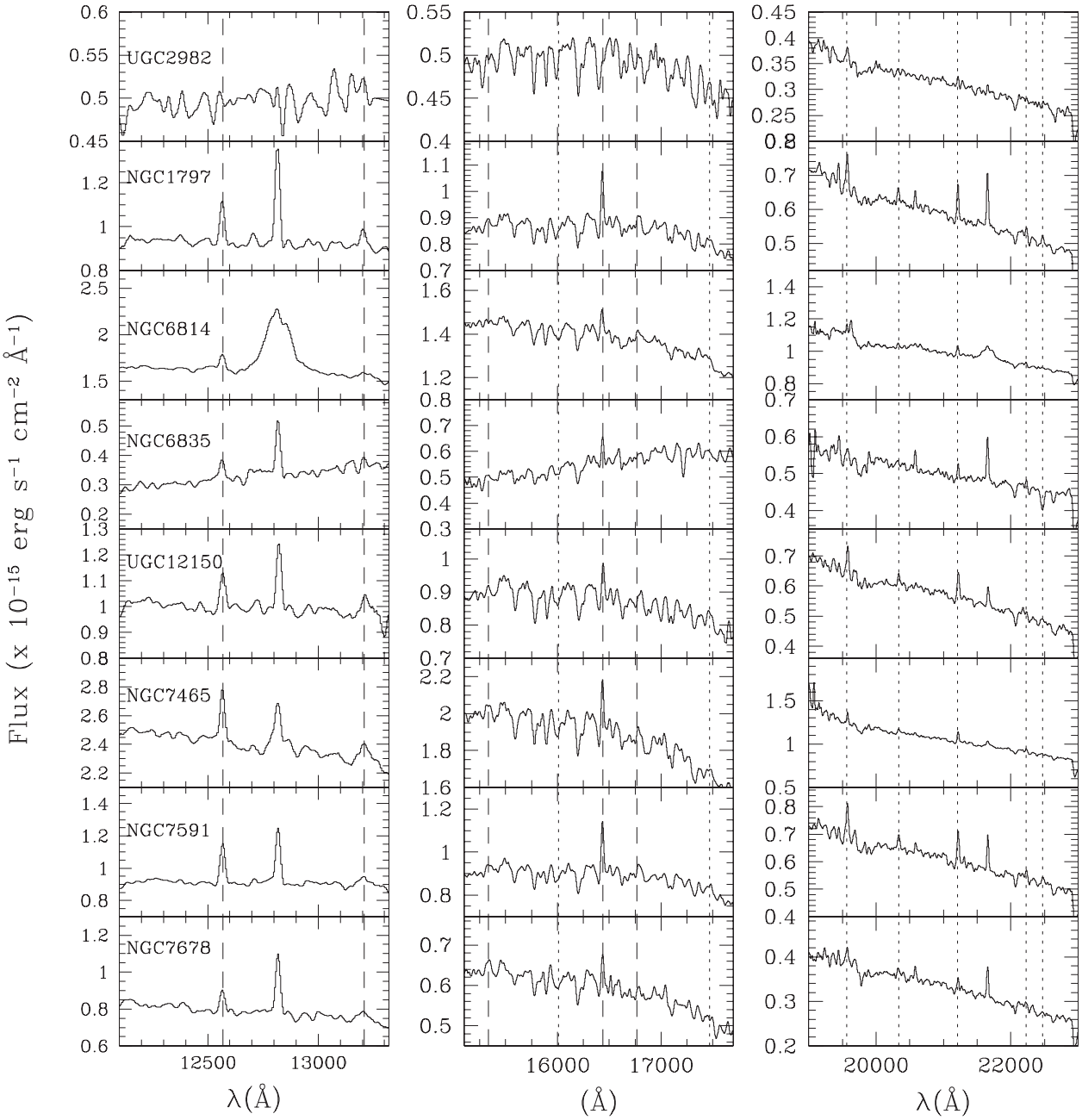

Figure 2. Same as Fig. 1 for the remaining objects.

the galaxy. According to literature results (Reunanen et al. 2002, 2003), it may be arranged in a disc-like structure. Further support of this hypothesis comes from the fact that, compared to SFGs, AGNs tend to have significantly broader [S III] than [Fe II] and H_2 (Fig. 4).

4 EXCITATION MECHANISMS OF THE H_2 LINES

As mentioned in the introduction, H_2-line ratios are used to discriminate among the dominant line excitation mechanisms. For example, Mouri (1994) suggested the use of the ratios 1–0 S(2) 2.033 μm/1–0 S(0) 2.223 μm versus 2–1 S(1) 2.247 μm/1–0 S(1) 2.121 μm to separate the mechanism exciting the H_2 emission. Fig. 5 shows this plot for the objects listed in Table 1 plus AGNs from Rodríguez-Ardila et al. (2004, 2005) and blue compact dwarf galaxies (BCGs) from Izotov & Thuan (2011). It can be seen from Fig. 5 that objects with different nuclear activities populate different regions of the diagram. Sy1s and SFGs tend to scatter over the plotted region, although Sy1s tend to have lower values of 2–1 S(1)/1–0 S(1) than SFGs, while Sy2 and LINERs are concentrated in a smaller region around the coordinates (0.1, 1.5). Note also that two BCGs are on the lower right of the plot.

Fig. 5 also shows results of model calculations found in the literature. The UV-excited low-density gas models of Black & van Dishoeck (1987) occupy the region indicated by the orange filled circle on the right, while the UV-excited high-density models of Sternberg & Dalgarno (1989) occupy the region indicated by the green box on the left. Models of X-ray-irradiated gas of Lepp & McCray (1983) are indicated by purple stars. The cyan star is a model of shock by Kwan (1977). Maloney et al. (1996) showed that for

Table 2. FWHM (in km s^{-1}) corrected for instrumental resolution. This correction was applied for lines with FWHM > 500 km s^{-1}. Lines with smaller values were reported as unresolved (FWHM = 360 km s^{-1}).

Source	[S III] 9530 (Å)	[Fe II] 1.2570 (μm)	H_2 1.9570 (μm)	H_2 2.0332 (μm)	H_2 2.1213 (μm)
NGC 23	435	563	492	360	360
NGC 520	–	–	360	360	360
NGC 660	612	402	390	360	360
NGC 1055	–	–	–	–	–
NGC 1134	–	–	–	–	–
NGC 1204	562	301	360	360	360
NGC 1222	500	447	601	360	360
NGC 1266	–	632	360	360	360
UGC 2982	–	–	648	360	360
NGC 1797	573	285	360	360	360
NGC 6814	717	583	368	360	360
NGC 6835	–	499	876	360	360
UGC 12150	611	508	527	360	360
NGC 7465	557	492	360	390	360
NGC 7591	669	367	666	363	360
NGC 7678	746	360	360	360	360

Note. The uncertainty associated with the FWHM is ∼30 km s^{-1} (for details see the text).

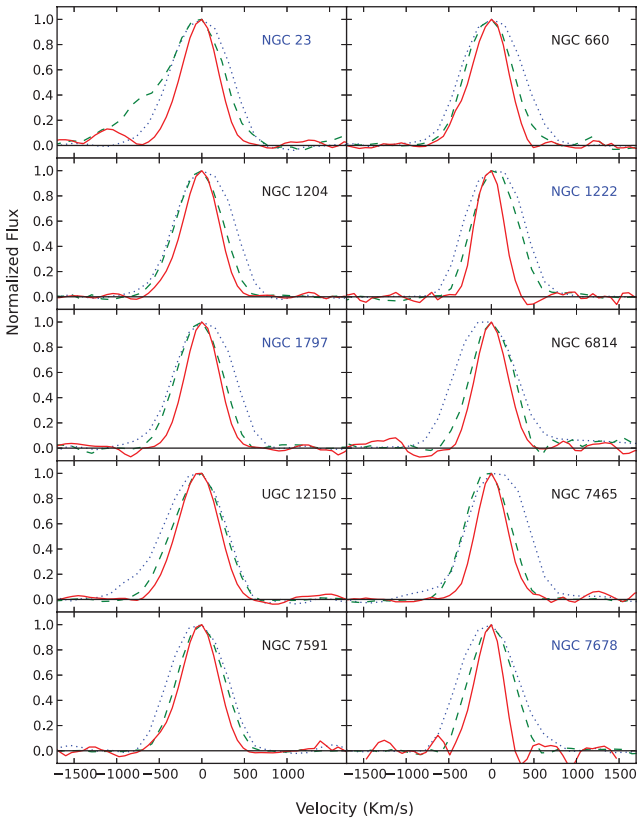

Figure 3. Observed line profiles of [S III] 9531Å (dotted blue line), [Fe II] 1.257 μm (dashed green line) and H_2 2.122 μm (full line). SFGs are labelled in blue colour.

X-ray-irradiated molecular gas, the 2–1 S(1)/1–0 S(1) ratio is $\lesssim$0.3 (∼0.1 in regions where the line 1–0 S(1) is more intense). Dors et al. (2012) calculated the ratios with the photoionization code CLOUDY for AGN models. They found that heating by X-rays produced

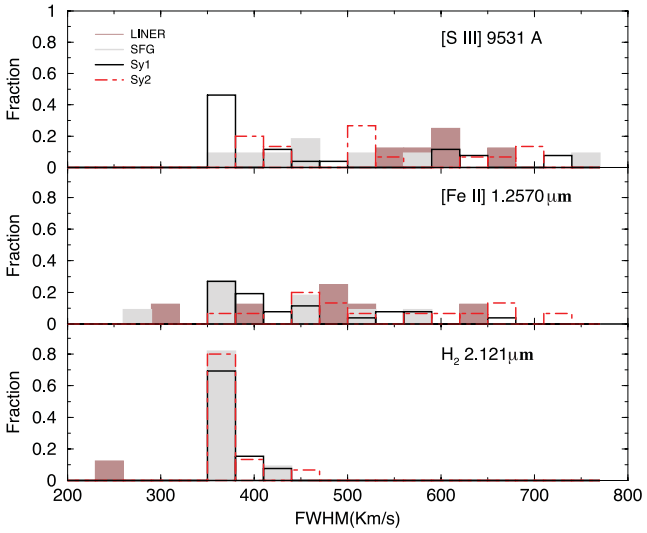

Figure 4. Histogram showing the FWHM distribution for LINERs, SFGs and Seyferts (the latter from Rodríguez-Ardila et al. 2004, 2005). The measurements for Seyferts were taken from Rodríguez-Ardila et al. (2004, 2005).

by active nuclei is a common and very important mechanism of H_2 excitation. Shock models by Kwan (1977) give 2–1 S(1)/1–0 S(1) = 0.092 and 1–0 S(2)/1–0 S(0) = 0.87, while Hollenbach & McKee (1989) find ratios in the range of 0.3–0.5 for the 2–1 S(1)/1–0 S(1) ratio.[3]

The observed ratios are not reproduced by any of pure low-density UV, high-density UV, X-rays or shock models only. Different processes may be more important in different objects. Moreover, a mixture of these processes is likely to be exciting the molecule in both AGNs and SBs. Here we will focus our discussion on the excitation due to a radiation source (i.e. no shock excitation).

The models of Sternberg & Dalgarno (1989) and Black & van Dishoeck (1987) only consider UV radiation (E < 13.6 eV). On the other hand, the models of Maloney et al. (1996) only consider X-ray radiation ($E \gtrsim$ 100 eV). Lepp & McCray (1983) presented very complete models and took a wider energy range into account, but they only calculated two models. Dors et al. (2012) obtained models for a single value of gas density ($n_H = 10^4$ cm^{-3}) and their calculations stopped when the temperature fell to $T = 1000$ K, missing an important part of the H_2 emission, where the X-rays may be of great importance (see the discussion of Fig. 8 and Aleman & Gruenwald 2011).

Here we present new calculations of the H_2 IR emission lines produced with a photoionization numerical code. These calculations are an improvement over the previously mentioned calculations, since they consider the spectrum from the IR up to X-rays ($10^{-5} \lesssim E \lesssim 1$ keV), and they run from the inner and more ionized zones to the outer and more neutral zones, where T decreases to 100 K. Processing of the radiation in the inner gas shells is done in a self-consistent way and the microphysics of H_2 is included in detail. The models are described below (Section 4.1). In Section 4.2, we compare the model and observed H_2-line ratios, with the aim of studying the excitation mechanism of these lines.

[3] This ratio is not indicated in Fig. 5 because the authors did not provide the corresponding 1–0 S(2)/1–0 S(0) ratios.

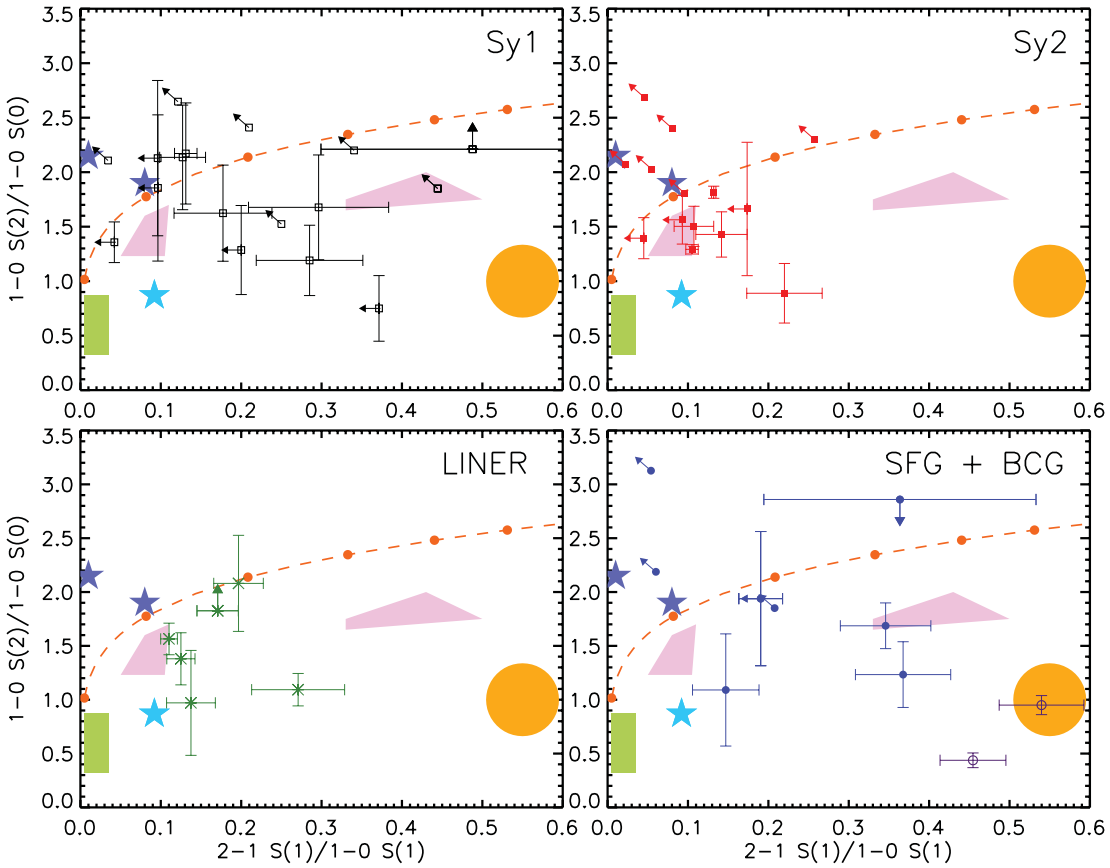

Figure 5. Objects with different nuclear activities populate different regions of the H_2 1–0 S(2) 2.033 μm/1–0 S(0) 2.223 μm versus 2–1 S(1) 2.247 μm/1–0 S(1) 2.121 μm diagnostic diagram. Different types of nuclear activities are shown in each plot as follows: Sy1, quasi-stellar object and NLSy1 (black open squares); Sy2 (red filled squares); LINERs (green asterisks); SFGs (blue filled circles) and BCGs (purple open circles). The orange dashed curve represents the ratios for an isothermal and uniform density gas distribution; each dot represents the temperatures from 1000 to 6000 K, in steps of 1000 K, from left to right. The orange circle on the right covers the locus of the non-thermal UV excitation models of Black & van Dishoeck (1987), while the green box (on the left) covers the locus of the thermal UV excitation models of Sternberg & Dalgarno (1989). Purple stars are thermal X-ray models of Lepp & McCray (1983) and the cyan star is a model of shock by Kwan (1977). Dors et al. (2012) models are indicated by the two pink polygons.

4.1 Models

We calculated the intensity of H_2 emission lines of AGNs using the one-dimensional photoionization code AANGABA (Gruenwald & Viegas 1992). The H_2 microphysics is included in detail in the code. To calculate the intensity of H_2 IR lines, the density and the population of the H_2 electronic ground-state rovibrational levels that originate the emission must be known. The density of H_2 is calculated assuming the chemical and ionization equilibrium between this molecule and the other H-bearing species (H^0, H^+, H^-, H_2^+ and H_3^+; see Aleman & Gruenwald 2004). The code includes over 40 different reactions of formation and destruction of these species. The population of the H_2 rovibrational levels of the three lowest electronic bound states is calculated by assuming statistical equilibrium (i.e. the total population rate of a level is equal to the total depopulation rate). The population of the electronic ground level takes into account the radiative and collisional excitation and de-excitation mechanisms, as well as the possibility that H_2 is produced or destroyed in any given level. For upper electronic levels, only radiative electronic transitions between each upper state and the ground state are included, since this must be the dominant mechanism.

The population of excited H_2 rovibrational levels of the electronic ground state occurs mainly by electric dipole transitions to upper electronic states, with the absorption of a UV photon, followed by the subsequent decay to the ground state (with the emission of a UV photon), usually in a excited rovibrational level. This mechanism of H_2 excitation is called UV pumping. The decay to lower levels, through quadrupole transitions, produces fluorescence. Collisions with the dominant species of the gas may also be an important route of H_2 excitation. We included collisions of H_2 with the main components of the gas, i.e. H, H^+, He, H_2 and electrons.

The H_2 molecule is also included in the gas temperature calculation, which assumes thermal equilibrium. (The total input of energy in the gas is balanced by the total loss of energy per unit time and volume.) The relevant mechanisms of gain and loss of energy by the gas due to atomic species, dust and H_2 are taken into account. The gas-heating mechanisms are photoionization of atoms, atomic ions and H_2 by the primary and diffuse radiation, H_2 photodissociation (direct and two steps), H_2 formation on grain surfaces, by associative detachment, and by charge exchange with H, H_2 collisional de-excitation and photoelectric effect on dust surfaces. The gas-cooling mechanisms are emission of collisionally excited lines, radiative and dielectronic atomic recombination, thermal collisional atomic ionization, free–free emission, collisional excitation of H_2 destruction of H_2 by charge exchange with H^+, H_2 collisional dissociation, and collision of gas-phase particles with dust grains. More details on the calculation of the H_2 level population are found in Aleman & Gruenwald (2004, 2011).

Table 3. Model elemental abundance relative to H.

Element	Abundance	Element	Abundance
H	1.0	Mg	3.8×10^{-5}
He	9.8×10^{-2}	Si	3.5×10^{-5}
C	3.6×10^{-4}	S	1.6×10^{-5}
N	1.1×10^{-4}	Cl	3.2×10^{-7}
O	8.5×10^{-4}	Ar	3.6×10^{-6}
Ne	1.2×10^{-4}	Fe	4.7×10^{-5}

The emissivity of a line produced by de-excitation from a given level is the product of the population of that level by the Einstein coefficient of the transition and by the energy of the emitted photon. The emissivities of the H_2 IR lines are calculated for each point of the nebula. The intensities are calculated by integrating the emissivity over the nebular volume. The gas is assumed to be optically thin for the H_2 lines.

We assume a spherical distribution, uniform density and composition for gas and dust, and gas densities (n_H) from 10^3 to 10^5 cm^{-3}, which are typical for AGNs (Osterbrock 1989). Solar abundance is assumed for the elements in all models (Osterbrock 1989), with values (Table 3) obtained from Grevesse & Anders (1989). The chemical composition affects the processing of the radiation inside the cloud and, consequently, the ionization structure of the cloud, but this does not significantly affect the H_2 ratios, as shown by Dors et al. (2012).

The dust, in our models, is assumed to be composed of spherical graphite grains with optical properties taken from Draine & Lee (1984) and Laor & Draine (1993). Models were calculated for two different grain radii: 10^{-2} and 10^{-1} μm, typical interstellar values according to Li (2007) and Mathis, Rumpl & Nordsieck (1977). As shown in Aleman & Gruenwald (2004), the dust particle size is more important for the H_2 density than the grain type. The dust-to-gas mass ratio (M_d/M_g) is assumed constant in all models. Models were calculated for $M_d/M_g = 10^{-3}$ and 10^{-2}, average values for planetary nebulae and the interstellar medium (Lenzuni, Natta & Panagia 1989; Stasińska & Szczerba 1999; Tielens 2005).

In our models, the spectrum of an AGN is approximated by a power law, i.e. $L = CE^{-\alpha}$, where E is the photon energy, L is the number of photons per unit time per unit of energy emitted by the source and α is the spectral index. The constant C roughly indicates the radiation field intensity. It is usually defined in terms of the ionization parameter, which is the ratio of the amount of hydrogen ionizing photons incident on the inner border of the cloud to the density of H atoms of the cloud. The ionization parameter (U) is then

$$U = \frac{Q_H}{4\pi R_{in}^2 n_H c},$$

where n_H is the numerical H density of the cloud, R_{in} is the internal radius of the cloud, Q_H is the number of hydrogen ionizing photons emitted by the ionizing source per unit of time and c is the speed of light. U values between 10^{-4} and 10^{-1} are inferred from the observations of the NLR of AGNs (e.g. Osterbrock 1989). In this paper, we use models for average U values (0.1, 0.01 and 0.001). The shape of the UV to X-ray spectral energy distribution (SED) can differ among AGNs (Prieto et al. 2010), a range well represented by spectral indices from 1.0 to 1.5, which we use in our models.

For comparison, we also include models with a SB-like spectrum. For such models, we assume that the ionizing spectrum has the shape given by Riffel et al. (2008b), which represents the underlying stellar population of the SB galaxy NGC 7714. We scale the spectrum to study a different number of ionizing photons. The models range from $\log(Q_H) = 52$ to 54, to cover SB values (Leitherer et al. 1995). We study the same range of gas and dust parameters as that for AGNs.

Our models show that the bulk of the H_2 NIR emission in AGNs is produced in the warm region of the gas, so we use $T \gtrsim 100$ K as the stop criterion for the models. For SBs, there is a non-negligible contribution from gas with $T < 100$ K in some cases, so the stop criterion is $T \gtrsim 50$ K.

4.2 H_2 diagnostic diagram: observations versus models

Fig. 6 shows the H_2-line ratios resulting from our AGN models and from observations. Similarly, Fig. 7 depicts the comparison of our SB models with observations. The observational data and the results of previous models shown in Fig. 5 are also included in the plots of Figs 6 and 7 for comparison.

Our models with typical AGN parameters can reproduce most of the observed values (including the SFGs), while SB models only account for a fraction of the SFGs and BCGs and subsample of the AGNs with high 1–0 S(2)/1–0 S(0). Our models confirmed that the H_2 excitation in AGNs is most likely produced in a gas irradiated by a spectrum rich in high-energy photons, while for the SBs the H_2 excitation could be due to SB-like spectra or by power-law spectra as can be seen in Figs 6 and 7. Models with a hard incident spectrum (i.e. with a large amount of high-energy photons or a lower α value) tend to have lower 2–1 S(1)/1–0 S(1) ratios than AGN models with soft spectra or SB models. The region around the coordinates (0.15, 1.5) on these plots is densely populated with Seyfert galaxies and LINERs. For $\alpha = 1.0$, only models with $n_H < 10^4$ cm^{-3} can reproduce the observations. Models with $\alpha = 1.5$ can reproduce the observations, with the exception of the dense ($n_H \sim 10^5$ cm^{-3}) $U = 0.1$ models. Alternatively, if the density of the cloud is $n_H \sim 10^5$ cm^{-3}, then it becomes thinner than our models, i.e. it has only gas at temperatures higher than 500 K (see the paragraph below). The observations around the coordinates (0.12, 1.5) can only be reproduced by models with $n_H \sim 10^3$ cm^{-3}. It is worth mentioning that the H_2-line ratios remain essentially unchanged if we consider an average AGN ionizing spectrum like the one used by Korista et al. (1997) or an equivalent power law. For the latter we mean an SED that produces approximately the same far-UV-(5 eV)-to-X-ray-(2 keV)-flux ratio. The Korista et al. (1997) SED, for example, is equivalent to a single power law with a spectral index of 1.4. As an example, one of our models with a spectral index of 1.5 gives the ratios 1–0 S(2)/1–0 S(0) = 1.252 and 2–1 S(1)/1–0 S(1) = 0.523, while a model with the same parameters plus the Korista et al. (1997) SED gives very similar results for 1–0 S(2)/1–0 S(0) = 1.174 and 2–1 S(1)/1–0 S(1) = 0.566.

The increase of the depth in the cloud also affects significantly the line ratios as can be seen in Fig. 8. In general, for increasing depth both ratios decrease towards lower values, initially following the local thermodynamic equilibrium (LTE) high temperature solutions (dashed curve) and then following a path that depends on object properties. It can clearly be observed in this figure that the ratios are significantly affected if the models run only for $T \geq 1000$ K (marked with red stars), thus, affecting model predictions.

The diagrams show that several factors, besides the radiation source, compete for the determination of H_2-line ratios. Gas and dust density, grain size, and the shape and luminosity of the central source spectra are the most important. For example, Fig. 6 shows that AGN models with high gas density tend to have low 1–0 S(2)/1–0 S(0) and 2–1 S(1)/1–0 S(1) ratios, reflecting an emission spectrum

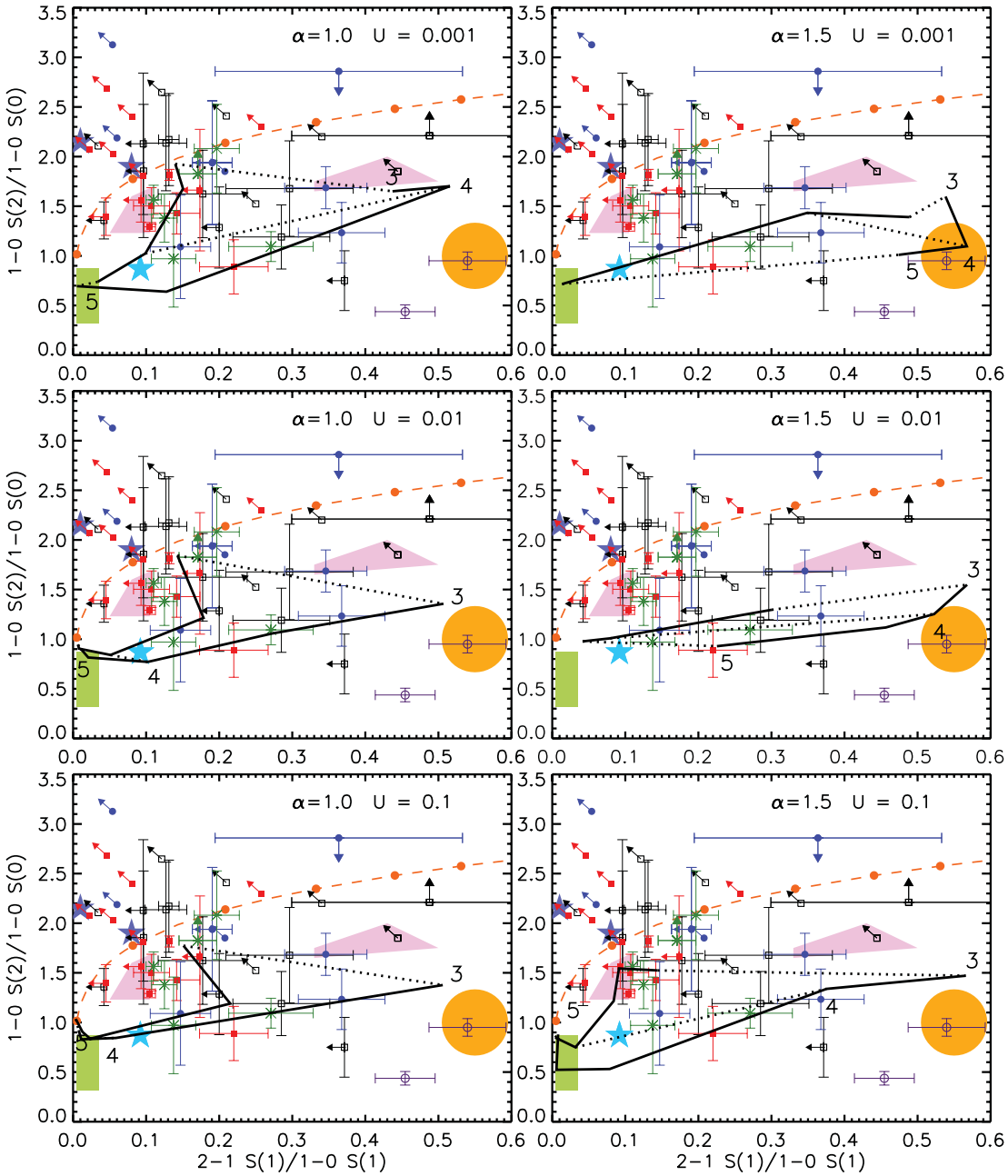

Figure 6. H_2 diagnostic diagram: comparing AGN models and observations. The symbols represent observations, the polygons represent models found in the literature, and the dashed curve represents the ratios for an isothermal and uniform gas density distribution; they follow the same notation as in Fig. 5. Calculated ratios are shown in each panel as solid lines. Each panel shows AGN models for a different power-law spectrum, with the ionization parameter U and the spectral index α as indicated. Each curve connects models for a dust grain size, $a_g = 10^{-1}$ (left-hand curve) and 10^{-2} μm (right-hand curve), where the gas density is varied. Dotted lines connect models of the same density for log $n_H = 3$, 4 and 5. These models assume that the cloud is at 1 pc from the central source.

dominated by collisions, as discussed by Sternberg & Dalgarno (1989). Values obtained by Kwan (1977) for shock regions are similar to our densest AGN models. For SBs, high-density models also tend to have low values of 1–0 S(2)/1–0 S(0), but the exact behaviour of 2–1 S(1)/1–0 S(1) with density also depends on other properties, as discussed below.

Since we assume a constant dust-to-gas ratio (and not the density of grains), increasing the gas density also increases proportionally the amount of dust. As shown in Fig. 7, increasing just the dust-to-gas ratio (keeping n_H constant) diminishes the 1–0 S(2)/1–0 S(0) ratio, but not necessarily 2–1 S(1)/1–0 S(1). We show only SB models with different dust densities, but the effect of increasing dust density on AGN models is similar to that on SB models.

As previously mentioned, dust grain size also plays an important role in H_2-line ratios. Models with smaller dust grains have smaller 2–1 S(1)/1–0 S(1) ratios. Assuming a constant dust-to-gas ratio, the optical depth due to dust and the H_2 formation rate are inversely proportional to the grain size, as shown in Aleman & Gruenwald (2004). For these reasons, more H_2 is produced in models with smaller grains.

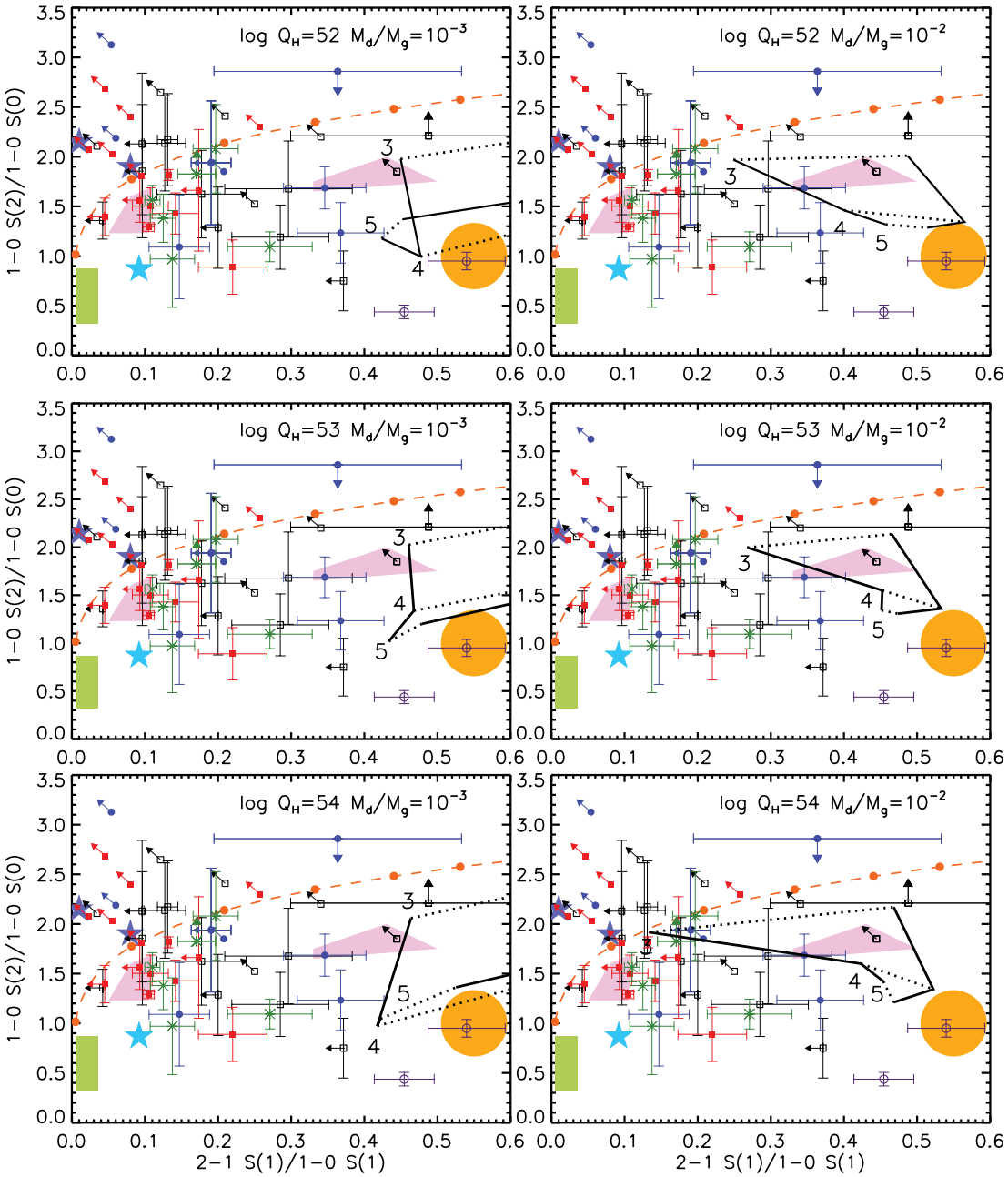

Figure 7. Same as Fig. 6, but for SB models. Calculated ratios are shown in each panel as solid lines, connecting models for different gas density. In each panel, the leftmost curve is for models with the dust grain size $a_g = 10^{-1}$ and the rightmost for 10^{-2} μm. Each panel shows SB models for different number of H ionizing photons (Q_H) and the dust-to-gas ratio (M_d/M_g). Q_H is given in photons s^{-1}. Dotted lines connect models of the same density for log $n_H = 3$, 4 and 5. These models assume that the cloud is at 1 pc from the central source.

4.3 H_2 excitation temperatures and masses

As stated in Rodríguez-Ardila et al. (2005), an alternative way to determine the mechanism driving the molecular gas excitation is to derive the rotational and vibrational temperatures for the H_2. A gas dominated by thermal excitation has similar rotational and vibrational temperatures (as expected for a gas in LTE) while fluorescent excitation is characterized by a high vibrational temperature and a low rotational temperature. For more details see Rodríguez-Ardila et al. (2005, and references therein).

The values of T_{vib} and T_{rot} can be calculated using the fluxes of the observed H_2 lines together with the expressions (Reunanen et al. 2002) $T_{vib} \cong 5600/\ln(1.355 \times I_{1-0S(1)}/I_{2-1S(1)})$ and $T_{rot} \cong -1113/\ln(0.323 \times I_{1-0S(2)}/I_{1-0S(0)})$. The derived values are presented in Table 5. It can be observed from that table and from Rodríguez-Ardila et al. (2005, table 4) that AGNs and LINERs tend to have similar values of T_{vib} and T_{rot}, while in the case of SFGs (NGC 23, NGC 520, NGC 34, NGC 1614 and NGC 7714, the latter three are from Rodríguez-Ardila sample) the T_{vib} tends to be higher than T_{rot}.

In addition to the excitation temperature, the fluxes of Table 4 also allow us to compute the mass of hot H_2 emitting the 1–0S(1) 2.121 μm line by means of the equation $m_{H_2} \simeq 5.0875 \times 10^{13} D^2 I_{1-0S(1)}$ (Reunanen et al. 2002).

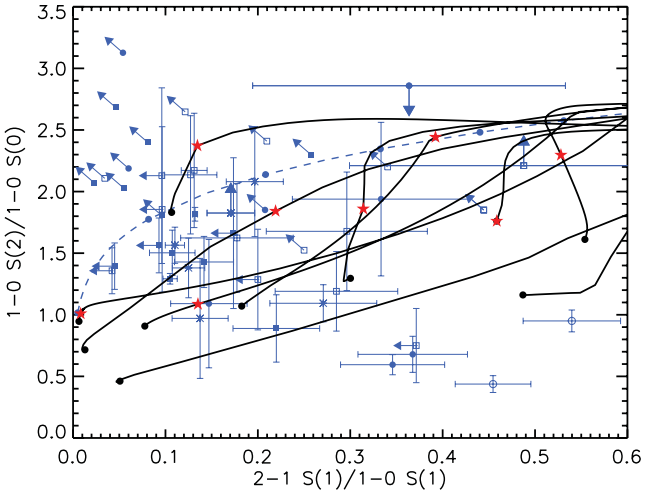

Figure 8. Behavior of the ratio 1–0 S(2)/1–0 S(0) versus 2–1 S(1)/1–0 S(1) with the distance from the inner border of the cloud, for several AGN models. Each solid curve represents a model, with distance increasing from right to left. The red stars and black dots over these curves indicate the stop criterion of $T = 1000$ and 100 K, respectively. Dots are observations and the dashed curve represents the ratios for an isothermal and uniform gas distribution as shown in Figs 6 and 7.

The mass of this hot H_2 for our galaxy sample is listed in Table 5. They were calculated assuming $T = 2000$ K, a transition probability $A_{S(1)} = 3.47 \times 10^{-7}$ s^{-1} (Turner, Kirby-Docken & Dalgarno 1977), the population fraction in the $v = 1$, $J = 3$ level $f_{v=1,J=3} = 0.0122$ (Scoville et al. 1982) and the intrinsic flux of H_2 2.121 μm, $I_{1-0S(1)}$. The extinction coefficient, C_{ext}, is calculated by assuming an intrinsic value of 5.88 for the flux ratio Paβ/Brγ (Osterbrock 1989, case B). As can be observed in Table 5 and in Rodríguez-Ardila et al. (2005), the mass of the hot H_2 is very similar for all activity types. The fraction of molecular mass present in the nuclear region and emitting in the NIR is a very small fraction of the warm molecular mass expected to be present in the galaxy centre (up to 10^{10} M$_\odot$, Young & Devereux 1991, for example) and is not related to activity type.

Table 5. Extinction coefficient, molecular gas mass, vibrational and rotational temperatures.

Source	C_{ext}	H_2 mass (M$_\odot$)	T_{vib} (K)	T_{rot} (K)
NGC 23	–	–	2521 ± 469	1067 ± 601
NGC 520	–	–	4115 ± 279	1832 ± 159
NGC 660	0.69	161 ± 5	2704 ± 240	2108 ± 208
NGC 1055	–	–	–	–
NGC 1134	–	–	–	–
NGC 1204	0.59	1991 ± 57	2912 ± 256	2776 ± 270
NGC 1222	0.21	67 ± 7	< 2856	2373 ± 399
NGC 1266	1.35	7189 ± 132	2232 ± 154	1631 ± 118
UGC 2982	–	–	–	–
NGC 1797	0.54	1606 ± 56	4293 ± 271	1209 ± 307
NGC 6814	0.00	56 ± 19	3607 ± 381	1165 ± 343
NGC 6835	0.98	201 ± 6	–	–
UGC 12150	0.43	3227 ± 97	2444 ± 363	960 ± 630
NGC 7465	0.47	323 ± 34	2362 ± 227	1378 ± 222
NGC 7591	0.51	2638 ± 82	3478 ± 361	1069 ± 174
NGC 7678	0.28	170 ± 17	4225 ± 806	–

Overall, the diagnostic diagrams presented in Figs 6 and 7 allow us to distinguish fairly well between the H_2 excitation mechanisms (collisional or UV pumping). However, it is not straightforward to distinguish between different classes of sources (e.g. AGN or SB), as discussed in the previous subsection. Alternatively, mechanisms may dominate the H_2 excitation in different regions in the same object. As the emission lines are integrated along the line of sight, we observe a combination of such processes. As can be seen in Figs 6 and 7, both collisional and UV pumping excitations may play an important role not only in AGNs but also in SFGs. This is further supported by the similarity between the vibrational and rotational temperatures of H_2 in some objects, and the tendency of T_{vib} to be higher than T_{rot} in others (see Table 5). For example, in SFGs, the thermal processes may dominate the excitation of the gas irradiated by supernova remnants (SNRs) or very hot stars. In this case, the H_2 emission is due to X-ray excitation, which would favour vibrational transitions over rotational transitions (Rodríguez-Ardila et al. 2005). Mouri (1994) showed that SNRs lies very close to the thermal curve in these diagnostic diagrams (see their fig. 1).

Table 4. Fluxes of atomic and molecular lines for our sample, in units of 10^{-15} erg cm^{-2} s^{-1}, measured in the sample.

Source	[Fe II] 1.2570 μm	Paβ 1.2820 μm	[Fe II] 1.6444 μm	H_2 1.9570 μm	H_2 2.0332 μm	H_2 2.1213 μm	H_2 2.2230 μm	H_2 2.2470 μm	Brγ 2.1650 μm
NGC 23	10.50 ± 0.87	–	14.20 ± 3.46	20.20 ± 4.60	4.94 ± 0.57	10.00 ± 1.26	4.53 ± 2.10[a]	1.47 ± 0.37	0.00 ± 0.00
NGC 520	–	–	3.87 ± 0.14	2.41 ± 0.39	1.13 ± 0.10	2.40 ± 0.18	0.67 ± 0.06	0.83 ± 0.12	6.67 ± 0.19
NGC 660	13.90 ± 0.65	29.0 ± 0.60	15.70 ± 0.90	8.87 ± 0.80	3.67 ± 0.56	6.91 ± 0.77	<2.01	1.18 ± 0.12[a]	16.60 ± 0.71
NGC 1055	–	–	–	–	0.00 ± 0.00	–	–	–	–
NGC 1134	–	–	–	–	0.00 ± 0.00	–	–	–	–
NGC 1204	5.16 ± 0.2	12.10 ± 0.20	6.51 ± 0.36	4.17 ± 0.51	1.81 ± 0.34	3.61 ± 0.25	0.87 ± 0.09	0.71 ± 0.10	5.88 ± 0.27
NGC 1222	6.32 ± 0.43	28.20 ± 0.37	4.65 ± 0.18	1.95 ± 0.34	0.95 ± 0.14	0.84 ± 0.12	0.49 ± 0.14	<0.16	6.98 ± 0.073
NGC 1266	3.19 ± 0.51	0.75 ± 0.08	2.90 ± 0.38	15.10 ± 0.47	5.10 ± 0.44	13.70 ± 0.25	3.26 ± 0.12	1.51 ± 0.14	1.40 ± 0.33
UGC 2982	–	–	–	1.79 ± 0.48	0.61 ± 0.08[a]	0.60 ± 0.02[a]	–	–	0.80 ± 0.036
NGC 1797	5.04 ± 0.25	12.10 ± 0.26	4.65 ± 0.47	4.10 ± 0.51	1.48 ± 0.30	3.21 ± 0.28	1.20 ± 0.17	1.18 ± 0.16	5.33 ± 0.09
NGC 6814	4.64 ± 0.52	3.53 ± 0.57	5.53 ± 0.48	3.36 ± 0.54	1.25 ± 0.20	2.14 ± 0.20	1.05 ± 0.23	0.61 ± 0.13	0.52 ± 0.32
NGC 6835	2.06 ± 0.23	4.86 ± 0.19	3.24 ± 0.08	3.33 ± 0.44	0.85 ± 0.05	1.34 ± 0.21	0.65 ± 0.18[a]	–	4.66 ± 0.25
UGC 12150	4.73 ± 0.33	7.86 ± 0.30	3.56 ± 0.18	5.25 ± 0.05	1.65 ± 0.07	4.00 ± 0.13	1.70 ± 0.85[a]	0.55 ± 0.12[a]	2.88 ± 0.13
NGC 7465	11.8 ± 0.66	9.57 ± 2.61	9.20 ± 0.28	4.33 ± 0.16	2.36 ± 0.39	3.92 ± 0.27	1.71 ± 0.10	0.49 ± 0.06	3.75 ± 0.69
NGC 7591	6.80 ± 0.21	9.74 ± 0.21	6.05 ± 0.60	8.17 ± 0.26	2.46 ± 0.20	4.80 ± 0.36	2.25 ± 0.25	1.30 ± 0.26	4.07 ± 0.052
NGC 7678	3.28 ± 0.49	9.20 ± 0.51	3.09 ± 0.21	1.45 ± 0.10	2.03 ± 0.20	0.88 ± 0.14	>0.71	0.32 ± 0.14	2.56 ± 0.15

[a] Affected by telluric absorption.

In the case of UV excitation by stars, the effective optical depth of the nebula, a non-thermal signature, will be determined if the ratios reflect the domination of a thermal or a non-thermal process (Sternberg & Dalgarno 1989).

5 NUCLEAR ACTIVITY FROM NIR EMISSION LINES

Since the H_2 and [Fe II] lines are common features in a wide variety of sources, it is interesting to investigate how these emission lines are compared in objects with different degrees of nuclear activities. A diagram involving the line ratios H_2 2.121 μm/Brγ and [Fe II] 1.257 μm/Paβ was proposed by Larkin et al. (1998) in a study of LINERs and other emission-line objects, including a few Seyferts. They reported a strong linear correlation in the log–log plot of [Fe II]/Paβ versus H_2/Brγ, with SBGs displaying the lower values, Seyferts with intermediate ones and LINERs with the highest ratios. They suggested that [Fe II]/Paβ ∼1 and H_2/Brγ ∼3 mark the end of Seyfert-like nuclei and the beginning of LINER-like objects. Rodríguez-Ardila et al. (2004, 2005) confirmed such a diagram as a suitable means of separating emission-line objects by their degrees of activities in the NIR and proposed that AGNs are characterized by H_2 2.121 μm/Brγ and [Fe II] 1.257 μm/Paβ flux ratios between 0.6 and 2. SBGs/H II galaxies display line ratios <0.6, while LINERs are characterized by values higher than 2 for both ratios. However, the lack of an adequate number of objects precludes definitive conclusions in those studies.

Here, with a larger sample and most importantly a more adequate number of objects of each activity class, we may provide further support to the trend already observed. Fig. 9 presents the updated version of H_2 2.121 μm/Brγ × [Fe II] 1.257 μm/Paβ diagnostic diagram. The sample analysed here is composed of the objects listed in Table 1 plus some taken from the literature: AGNs from Rodríguez-Ardila et al. (2004, 2005), SFGs from Dale et al. (2004) and Larkin et al. (1998), LINERs, supernova remnants (SNRs) from Larkin et al. (1998) and BCGs from Izotov & Thuan (2011). As can be seen in Fig. 9, LINERs and AGNs are not clearly separated by such a diagram. However, our sample of LINERs is composed of luminous infrared galaxies (LIRGs), and the classification in Table 1 is based on optical emission-line diagrams, which are affected by reddening (see Rodríguez-Ardila et al. 2005, for example). Since LIRGs harbour large quantities of dust, we suggest that the LINERs lying within the region of AGNs may hide a Seyfert nucleus.

With our sample comprising ∼65 objects, we not only confirm the diagram (Fig. 9) as a discriminator of emission-line objects by their degrees of activities, but we also provide improved limits to the line ratios for each activity type. The limits are as follows: (i) SFGs [Fe II] 1.257 μm/Paβ $\lesssim$ 0.6 and H_2 2.121 μm/Brγ $\lesssim$ 0.4, (ii) AGNs 0.6 $\lesssim$ [Fe II] 1.257 μm/Paβ $\lesssim$ 2 and 0.4 $\lesssim$ H_2 2.121 μm/Brγ $\lesssim$ 6 and (iii) LINERs [Fe II] 1.257 μm/Paβ $\gtrsim$ 2 and H_2 2.121 μm/Brγ $\gtrsim$ 6.

As discussed in Rodríguez-Ardila et al. (2005) on a pure observational basis, the interpretation of Fig. 9 is not straightforward. For example, the correlation between H_2/Brγ and [Fe II]/Paβ may originate from the fact that H_2 and [Fe II] are mainly excited by the same mechanism, i.e. X-ray. In fact, it was shown very recently by Dors

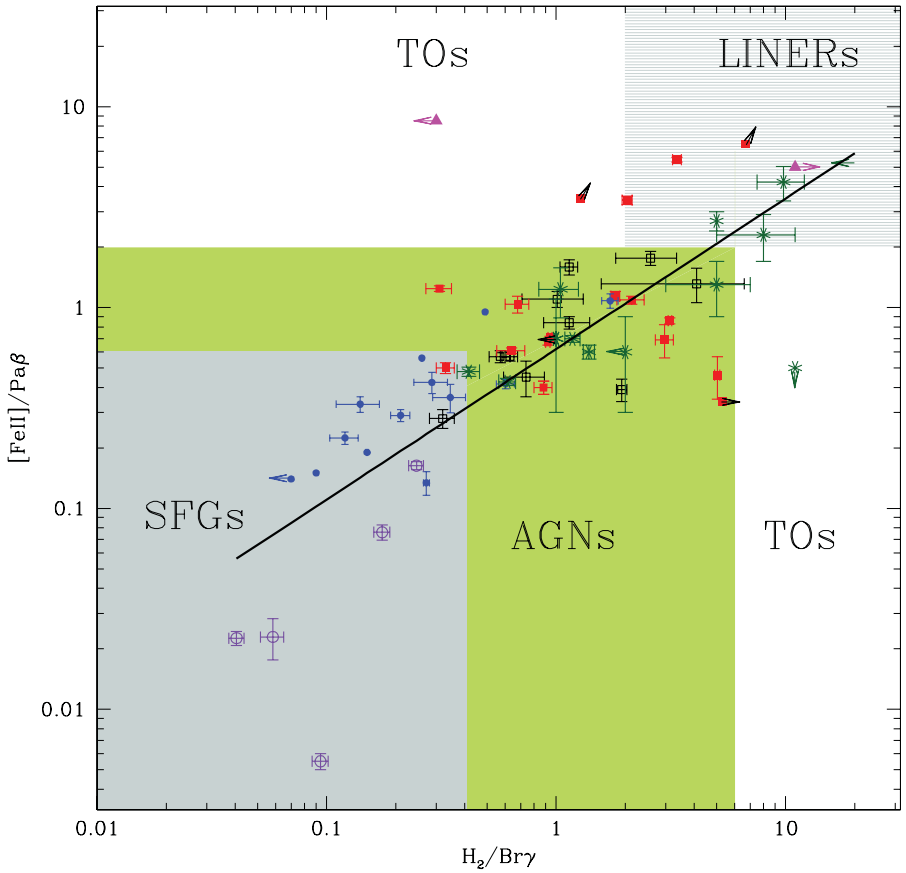

Figure 9. Diagnostic diagram: boxes are AGNs, Sy1 in black (open) and Sy2 in red (filled), asterisks are LINERs (green), filed circles are SFGs (blue), triangles (magenta) are SNRs and open circles are BCGs (violet). The solid line is [Fe II]/Paβ = 0.749(±0.072)H_2/Brγ − 0.207 ± 0.046 with the correlation coefficient = 0.80 and r^2 = 0.64.

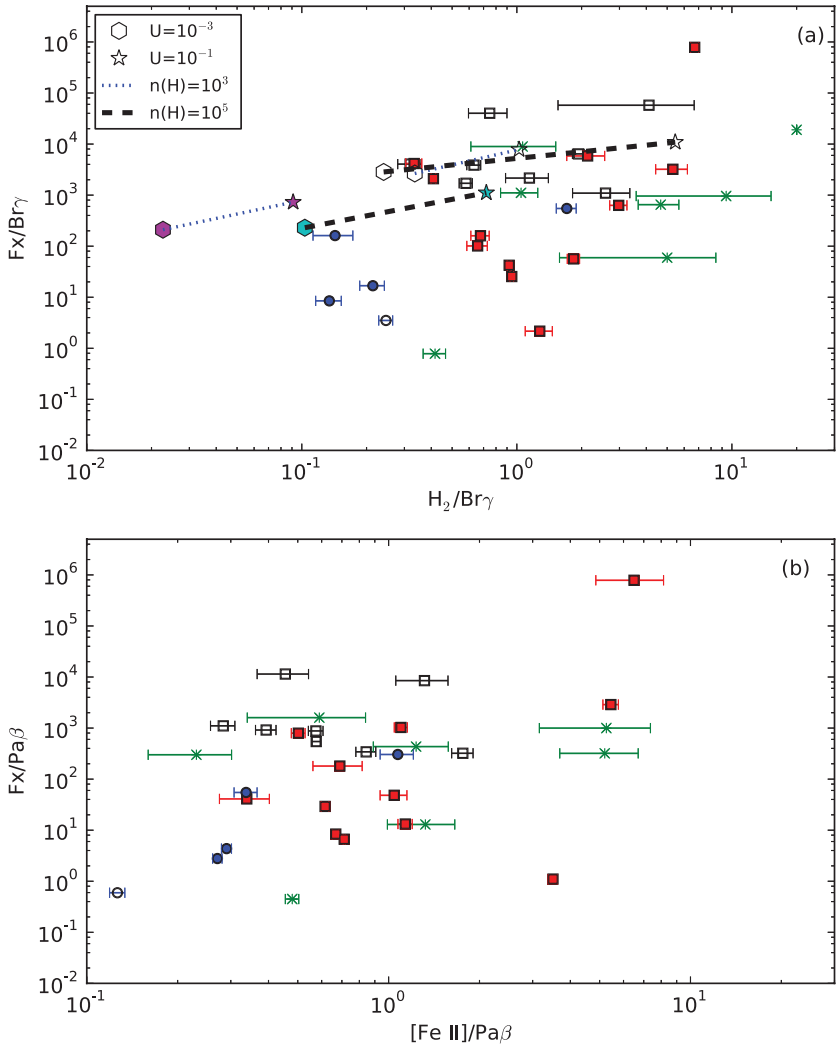

Figure 10. Hard X-ray flux versus emission-line ratios. The symbols for the observations are the same as in Fig. 9. Hexagons represent models with $U = 10^{-3}$ and stars with $U = 10^{-1}$ (open symbols are for $\alpha = 1$ and filled for $\alpha = 1.5$). Points joined by the dotted and dashed lines represent $n(\mathrm{H}) = 10^3$ and $n(\mathrm{H}) = 10^5$, respectively.

et al. (2012), using photodissociation models, that X-ray heating from the AGN is an important mechanism in the excitation of these NIR emission lines in AGNs (see Section 4). They also showed that a decrement in the X-ray content of the continuum source translates into a line weakening, and their models are no longer compatible with observations. However, X-ray heating is a plausible explanation for AGNs, but may not work for LINERs. Larkin et al. (1998), for example, argued that hard X-ray heating from a power law is a plausible mechanism to explain LINERs with low values of the [Fe II]/Paβ and H_2 2.121 μm/Brγ ratios. But it would not explain the high values (up to ∼7) observed in some objects. Nevertheless, the high [Fe II]/Paβ line ratios may be explained by the dependence of [Fe II]/Paβ on the Fe/O abundance and on the ionization parameter of the molecular gas, leading to high values for both ratios (Dors et al. 2012, see their fig. 1).

On the other hand, it has been recently proposed that it is unlikely that LINER emission lines are powered by photoionization by the low-luminosity AGN they harbour (Cid Fernandes et al. 2010; Eracleous, Hwang & Flohic 2010; Yan & Blanton 2012). This would rule out X-ray heating as the main mechanism driving the excitation of the NIR emission lines in LINERs. We investigated the role played by the hard X-ray (2–10 keV; F_x) radiation in [Fe II] and H_2 emission lines with diagrams involving F_x/Brγ versus H_2/Brγ ratios and F_x/Paβ versus [Fe II]/Paβ (Fig. 10). The X-ray fluxes were taken from the literature and are listed in Table 6. A mild correlation is observed for F_x/Brγ versus H_2/Brγ (Fig. 10a), indicating that the X-ray heating is an important mechanism in the molecular gas excitation. For a more objective assessment of the X-ray heating in our data, we included model predictions to Fig. 10a. It is clear that the explored parameter space overlaps the observed line ratios. In addition, the AGNs are better explained by $\alpha = 1$ and $U = 0.1$. It is also interesting that Sy1s require higher hydrogen gas densities than the other activity types, indicating that the molecular gas in Sy1s is denser. No correlation is observed for F_x/Paβ and [Fe II]/Paβ, and as for the diagram involving H_2/Brγ, no separation is observed between LINERs and Seyferts (Fig. 10). This result suggests that X-ray heating alone is not responsible for the observed sequence in Fig. 9. As shown by Dors et al. (2012), high values of [Fe II]/Paβ line ratios can be explained by the dependence on the Fe/O abundance. Thus, the observed sequence in Fig. 9 may be a consequence of the amount of X-ray photons together with abundance effect (i.e. in the case of LINERs powered by star

Table 6. Hard X-ray fluxes, in units of 10^{-13} erg cm^{-2} s^{-1}, taken from the literature.

Source	F_x (2–10 keV)	Reference
Sy1		
Mrk 334	80	Lutz et al. (2004)
NGC 7469	290	Lutz et al. (2004)
NGC 3227	75	Lutz et al. (2004)
NGC 4151	900	Lutz et al. (2004)
Mrk 766	300	Lutz et al. (2004)
NGC 4748	30	Landi et al. (2010)
NGC 5548	430	Lutz et al. (2004)
NGC 6814	300	Turner & Pounds (1989)
	Sy2	
ESO 428−G014	3.8	Lutz et al. (2004)
NGC 591	2	Guainazzi, Matt & Perola (2005)
Mrk 573	2.8	Guainazzi et al. (2005)
Mrk 1066	3.6	Guainazzi et al. (2005)
NGC 2110	430	Nandra et al. (2007)
NGC 7674	5	Lutz et al. (2004)
NGC 5929	79	Lutz et al. (2004)
Mrk 1210	250	Lutz et al. (2004)
NGC 5728	13.3	Shu et al. (2007)
Mrk 993	6.1	Guainazzi et al. (2005)
NGC 5953	0.06	Guainazzi et al. (2005)
NGC 1144	1100	Lutz et al. (2004)
	LINER	
NGC 5194	4.8	Cappi et al. (2006)
NGC 7743	0.44	González-Martín et al. (2009)
NGC 660	0.13	Filho et al. (2004)
NGC 7465	41.5	Guainazzi et al. (2005)
NGC 3998	84.2	Ueda et al. (2001)
NGC 7479	3.9	Ueda et al. (2005)
NGC 4736	19	Ueda et al. (2001)
	SFG	
NGC 34	39	Lutz et al. (2004)
NGC 7714	2.6	Ueda et al. (2005)
NGC 1614	3.6	Ueda et al. (2001)
NGC 3310	17.4	Ueda et al. (2001)
	BCDg	
Mrk 930	0.161	González et al. (2009)

formation, SN explosions would eject enriched material to the interstellar medium).

A detailed interpretation of the variation of these line ratios, from pure-SB-driven emission to LINER nuclei, is non-trivial. A possible scenario is that the different line ratios reflect different excitation mechanisms in the sense that they are able to describe a transition from an ionizing radiation powered by star formation to pure shock excitation driven by SNRs (Mazzalay et al. 2013). In such a case, the emission-line ratios observed in our LINER sample would be a combination of processes, from X-ray heating to star-formation/evolution. Since most LINERS have strong star formation (Table 1), the stars could provide the required electromagnetic or mechanical power to produce the observed line strengths. However, to clearly investigate this issue, a 3D simulation of the emitting gas would be needed (i.e. AGN in the centre + star formation in a volume). It is also worth mentioning that, in the case of star formation, the underlying stellar population would significantly affect the atomic hydrogen emission lines, thus affecting the observed line ratios (Larkin et al. 1998; Riffel et al. 2008b).

Another interesting point is the fact that Brγ is produced mostly inside the hydrogen-ionized region, while the H_2 emission originates in a warm semi-ionized region (Aleman & Gruenwald 2011) around the hydrogen recombination and in the photodissociation region, where H is mostly neutral. SFGs typically have lower 1–0 S(1)/Brγ ratios than AGNs. This may indicate that the region that produces the H_2 emission in AGNs is larger than in SBs, if we consider that AGN spectra are harder than that of SFGs. Harder ionization spectra may produce a more extended semi-ionized region (Aleman & Gruenwald 2004, 2007), which favours the formation and emission of H_2. In our models, the ratio H_2 1–0 S(1)/Brγ is within the range of $10^{-3} <$ H_2 1–0 S(1)/Brγ < 10 (see Section 4), with the higher ratios (>1) occurring in models with $\alpha = 1.0$ and the smallest values ($<10^{-2}$) occurring for $\alpha = 1.5$. (In fact, the emissions of these last objects are below the detection limit of our observations.) Furthermore, denser and/or dustier models typically have higher ratios. A more detailed discussion on these models will be made in a forthcoming work (Aleman et al., in preparation).

6 CONCLUDING REMARKS

We present NIR spectroscopy (0.8–2.4 μm) of seven SFGs and nine LINERs to discuss the distribution and excitation of the emitting H_2 and [Fe II] gas in emission-line galaxies. These data were analysed together with similar AGN data of two previous publications (Rodríguez-Ardila et al. 2004, 2005). The whole data set constitutes the most complete and homogeneous sample of such kind of objects observed in the NIR to date. Our main conclusions are as follows.

(i) H_2 is common within the inner few hundred parsecs of emission-line galaxies, regardless of type. However, the molecular gas follows different kinematics than that of the ionized gas, suggesting that the two emissions are not co-spatial. For example, it is clear that the H_2 lines are narrower than the forbidden lines, especially for [S III]. This could be interpreted as if the latter is broadened by the gravitational influence of the SMBH in the AGNs. Furthermore, LINERs tend to have [S III] significantly broader than [Fe II] and H_2 compared to SFGs. The fact that H_2 FWHM is unresolved in almost all objects implies that the molecular gas is probably not gravitationally bound to the SMBH but to the gravitational potential of the galaxy following a different kinematics than that of the classical NLR gas. In addition, IFU data and rotation curves derived for H_2 and published by other authors for objects in common with our sample support this hypothesis and point to a scenario where H_2 may be arranged in a disc-like structure on the galaxy plane.

(ii) We have computed new photoionization models for clouds ionized by AGNs and stars, which provided fluxes of the H_2 lines. We use a diagnostic diagram with H_2 IR line ratios to study the excitation mechanisms of H_2. The thermal excitation plays an important role not only in AGNs, but also in SFGs. This hypothesis is further supported by the similarity between the vibrational and rotational temperatures of H_2 in some objects, and the tendency of $T_{\rm vib}$ to be higher than $T_{\rm rot}$ in others. In SFGs, the importance of the thermal excitation may be associated with the presence of SNRs close to the region emitting H_2 lines.

(iii) With our extended sample, of 65 objects, we have confirmed that the diagram involving the line ratios H_2 2.121 μm/Brγ and [Fe II] 1.257 μm/Paβ is an efficient tool for separating emission-line objects according to their dominant degree of activity and

should be useful for classifying objects with hidden AGNs or highly reddened objects. We also provide improved limits to the line ratio intervals for each activity type, as follows: (1) SFGs [Fe II] 1.257 μm/Pa$\beta \lesssim 0.6$ and H_2 2.121 μm/Br$\gamma \lesssim 0.4$, (2) AGNs $0.6 \lesssim$ [Fe II] 1.257 μm/Pa$\beta \lesssim 2$ and $0.4 \lesssim H_2$ 2.121 μm/Br$\gamma \lesssim 6$ and (3) LINERs [Fe II] 1.257 μm/Pa$\beta \gtrsim 2$ and H_2 2.121 μm/Br$\gamma \gtrsim 6$,

(iv) A positive correlation is found in the diagnostic diagram involving the above ratios, interpreted as being a more likely an apparent correlation, since different mechanisms drive the production of either [Fe II] or H_2 according to the level of nuclear activity. It is not discarded that a combination of X-ray heating from the central source (in AGNs) plus shock heating (radio jet and NLR gas interaction) and/or SNRs can simultaneously drive the emission of [Fe II], supporting this correlation in LINERs and SFGs.

ACKNOWLEDGEMENTS

We thank an anonymous referee for valuable comments that helped to improve the text. RR thanks to FAPERGs (ARD 11/1758-5), CNPq (304796/2011-5) and Instituto Nacional de Ciência e Tecnologia em Astrofísica - INCT-A, funded by CNPq and FAPESP. ARA acknowledges CNPq (308877/2009-8) for partial support to this work. IA acknowledges support from CAPES/PRODOC and FAPESP (Proc. 2007/04498-2). OLD is grateful to the FAPESP for support under grant 2009/14787-7. This research has made use of the NASA/IPAC Extragalactic Database (NED) which is operated by the Jet Propulsion Laboratory, California Institute of Technology, under contract with the National Aeronautics and Space Administration.

REFERENCES

Aleman I., Gruenwald R., 2004, ApJ, 607, 865
Aleman I., Gruenwald R., 2011, A&A, 528, A74
Alloin D., Galliano E., 2002, A&A, 393, 43
Alonso-Herrero A., Rieke M. J., Rieke G. H., Ruiz M., 1997, ApJ, 482, 747
Balzano V. A., 1983, ApJ, 268, 602
Black J. H., van Dishoeck E. F., 1987, ApJ, 322, 412
Cappi M. et al., 2006, A&A, 446, 459
Cid Fernandes R., González Delgado R. M., Storchi-Bergmann T., Martins L. P., Schmitt H., 2005, MNRAS, 356, 270
Cid Fernandes R., Stasińska G., Schlickmann M. S., Mateus A., Vale Asari N., Schoenell W., Sodré L., 2010, MNRAS, 403, 1036
Cid Fernandes R. et al., 2004, ApJ, 605, 105
Condon J. J., Cotton W. D., Broderick J. J., 2002, AJ, 124, 675
Contini M., Radovich M., Rafanelli P., Richter G. M., 2002, ApJ, 572, 124
Dale D. A. et al., 2004, ApJ, 601, 813
Davies R. I., Sternberg A., Lehnert M. D., Tacconi-Garman L. E., 2005, ApJ, 633, 105
Davies R. I., Maciejewski W., Hicks E. K. S., Tacconi L. J., Genzel R., Engel H., 2009, ApJ, 702, 114
Dors O. L., Jr, Riffel R. A., Cardaci M. V., Hägele G. F., Krabbe A. C., Pérez-Montero E., Rodrigues I., 2012, MNRAS, 422, 252
Draine B. T., Lee H. M., 1984, ApJ, 285, 89
Eracleous M., Hwang J. A., Flohic H. M. L. G., 2010, ApJ, 711, 796
Ferruit P., Wilson A. S., Mulchaey J., 2000, ApJS, 128, 139
Filho M. E., Fraternali F., Markoff S., Nagar N. M., Barthel P. D., Ho L. C., Yuan F., 2004, A&A, 418, 429
Forbes D. A., Ward M. J., 1993, ApJ, 416, 150
González Delgado R. M., Cid Fernandes R., Pérez E., Martins L. P., Storchi-Bergmann T., Schmitt H., Heckman T., Leitherer C., 2004, ApJ, 605, 127
González-Martin O., Masegosa J., Márquez I., Guainazzi M., Jiménez-Bailón E., 2009, A&A, 506, 1107
Gonçalves A. C., Veron P., Veron-Cetty M.-P., 1998, A&AS, 127, 107
Goodrich R. W., Veilleux S., Hill G. J., 1994, ApJ, 422, 521
Gratadour D., Clénet Y., Rouan D., Lai O., Forveille T., 2003, A&A, 411, 335
Grevesse N., Anders E., 1989, in Waddington C. J., ed., AIP Conf. Ser. Vol. 183, Cosmic Abundances of Matter. Am. Inst. Phys., New York, p. 1
Gruenwald R., Viegas S. M., 1992, ApJS, 78, 153
Guainazzi M., Matt G., Perola G. C., 2005, A&A, 444, 119
Ho L. C., Filippenko A. V., Sargent W. L., 1997a, ApJS, 112, 315
Ho L. C., Filippenko A. V., Sargent W. L., Peng C. Y., 1997b, ApJS, 112, 391
Hollenbach D., McKee C. F., 1989, ApJ, 342, 306
Imanishi M., Dudley C. C., 2000, ApJ, 545, 701
Imanishi M., Wada K., 2004, ApJ, 617, 214
Ivanov V. D., Rieke G. H., Groppi C. E., Alonso-Herrero A., Rieke M. J., Engelbracht C. W., 2000, ApJ, 545, 190
Izotov Y. I., Thuan T. X., 2011, ApJ, 734, 82
Knop R. A., Armus L., Larkin J. E., Matthews K., Shupe D. L., Soifer B. T., 1996, AJ, 112, 81
Korista K., Baldwin J., Ferland G., Verner D., 1997, ApJS, 108, 401
Kwan J., 1977, ApJ, 216, 713
Landi R., Bassani L., Malizia A., Stephen J. B., Bazzano A., Fiocchi M., Bird A. J., 2010, MNRAS, 403, 945
Laor A., Draine B. T., 1993, ApJ, 402, 441
Larkin J. E., Armus L., Knop R. A., Soifer B. T., Matthews K., 1998, ApJS, 114, 59
Leitherer C., Ferguson H. C., Heckman T. M., Lowenthal J. D., 1995, ApJ, 454, L19
Lenzuni P., Natta A., Panagia N., 1989, ApJ, 345, 306
Lepp S., McCray R., 1983, ApJ, 269, 560
Li A., 2007, in Ho L. C., Wang J.-M., eds, ASP Conf. Ser. Vol. 373, The Central Engine of Active Galactic Nuclei. Astron. Soc. Pac., San Francisco, p. 561
Lutz D., Maiolino R., Spoon H. W. W., Moorwood A. F. M., 2004, A&A, 418, 465
Maloney P. R., Hollenbach D. J., Tielens A. G. G. M., 1996, ApJ, 466, 561
Mathis J. S., Rumpl W., Nordsieck K. H., 1977, ApJ, 217, 425
Mazzalay X. et al., 2013, MNRAS, 428, 2389
Mizutani K., Suto H., Maihara T., 1994, ApJ, 421, 475
Mouri H., 1994, ApJ, 427, 777
Mouri H., Kawara K., Taniguchi Y., 2000, ApJ, 528, 186
Müller Sánchez F., Davies R. I., Genzel R., Tacconi L. J., Eisenhauer F., Hicks E. K. S., Friedrich S., Sternberg A., 2009, ApJ, 691, 749
Nandra K., O'Neill P. M., George I. M., Reeves J. N., 2007, MNRAS, 382, 194
Neumayer N., Cappellari M., Reunanen J., Rix H.-W., van der Werf P. P., de Zeeuw P. T., Davies R. I., 2007, ApJ, 671, 1329
Oterbrock D. E., 1989, Astrophysics of Gaseous Nebulae and Galactic Nuclei. University Science Books, Mill Valley, CA
Pereira-Santaella M., Diamond-Stanic A. M., Alonso-Herrero A., Rieke G. H., 2010, ApJ, 725, 2270
Prieto M. A., Reunanen J., Tristram K. R. W., Neumayer N., Fernandez-Ontiveros J. A., Orienti M., Meisenheimer K., 2010, MNRAS, 402, 724
Quillen A. C., Alonso-Herrero A., Rieke M. J., Rieke G. H., Ruiz M., Kullarni V., 1999, ApJ, 527, 696
Rayner J. T., Toomey D. W., Onaka P. M., Denault A. J., Stahlberger W. E., Vacca W. D., Cushing M. C., Wang S., 2003, PASP, 155, 362
Reunanen J., Kotilainen J. K., Prieto M. A., 2002, MNRAS, 331, 154
Reunanen J., Kotilainen J. K., Prieto M. A., 2003, MNRAS, 343, 192
Riffel R. A., Storchi-Bergmann T., 2011a, MNRAS, 411, 469
Riffel R. A., Storchi-Bergmann T., 2011b, MNRAS, 417, 2752
Riffel R., Rodríguez-Ardila A., Pastoriza M. G., 2006a, A&A, 457, 61
Riffel R. A., Storchi-Bergmann T., Winge C., Barbosa F. K. B., 2006b, MNRAS, 373, 2
Riffel R. A., Storchi-Bergmann T., Winge C., McGregor P. J., Beck T., Schmitt H., 2008a, MNRAS, 385, 1129
Riffel R., Pastoriza M. G., Rodríguez-Ardila A., Maraston C., 2008b, MNRAS, 388, 803

Riffel R. A. et al., 2013, preprint (arXiv:1212.0395)
Rodríguez-Ardila A., Viegas S. M., 2003, MNRAS, 340, 33
Rodríguez-Ardila A., Pastoriza M. G., Viegas S. M., Sigut T. A. A., Pradhan A. K., 2004, A&A, 425, 457
Rodríguez-Ardila A., Riffel R., Pastoriza M. G., 2005, MNRAS, 364, 1041
Rosa Gonzlez D., Terlevich E., Jimnez Bailn E., Terlevich R., Ranalli P., Comastri A., Laird E., Nandra K., 2009, MNRAS, 399, 487
Schinnerer E., Eckart A., Tacconi L. J., 1999, ApJ, 524, L5
Schmitt H. R., Calzetti D., Armus L., Giavalisco M., Heckman T. M., Kennicutt R. C. Jr, Leitherer C., Meurer G. R., 2006, ApJ, 643, 173
Scoville N. Z., Hall D. N. B., Kleinmann S. G., Ridgway S. T., 1982, ApJ, 459, 535
Shi L., Gu Q. S., Peng Z. X., 2006, A&A, 450, 15
Shu X. W., Wang J. X., Jiang P., Fan L. L., Wang T. G., 2007, ApJ, 657, 167
Simpson C., Forbes D. A., Baker A. C., Ward M. J., 1996, MNRAS, 283, 777
Stasińska G., Szczerba R., 1999, A&A, 352, 297
Sternberg A., Dalgarno A., 1989, ApJ, 338, 197
Storchi-Bergmann T., Nemmen R. S., Spinelli P. F., Eracleous M., Wilson A. S., Filippenko A. V., Livio M., 2005, ApJ, 624, L13
Storchi-Bergmann T., McGregor P. J., Riffel R. A., Simões Lopes R., Beck T., Dopita M., 2009, MNRAS, 394, 1148
Storchi-Bergmann T., Simões Lopes R. D., McGregor P. J., Riffel R. A., Beck T., Martini P., 2010, MNRAS, 402, 819
Storchi-Bergmann T., Riffel R. A., Riffel R., Diniz M. R., Borges Vale T., McGregor P. J., 2012, ApJ, 755, 87
Sturm E., Lutz D., Verma A., Netzer H., Sternberg A., Moorwood A. F. M., Oliva E., Genzel R., 2002, A&A, 393, 821
Sturm E. et al., 2006, ApJ, 653, 13
Tielens A. G. G. M., 2005, The Physics and Chemistry of the Interstellar Medium. Cambridge Univ. Press, Cambridge
Turner T. J., Pounds K. A., 1989, MNRAS, 240, 833
Turner J., Kirby-Docken K., Dalgarno A., 1977, ApJS, 35, 281
Ueda Y., Ishisaki Y., Takahashi T., Makishima K., Ohashi T., 2001, ApJS, 133, 1
Ueda Y., Ishisaki Y., Takahashi T., Makishima K., Ohashi T., 2005, ApJS, 161, 185
Vacca W. D., Cushing M. C., Rayner J. T., 2003, PASP, 115, 389
Veilleux S., Kim D.-C., Sanders D. B., Mazzarella J. M., Soifer B. T., 1995, ApJS, 98, 171
Veilleux S., Goodrich R. W., Hill G. J., 1997, ApJ, 477, 631
Yan R., Blanton M. R., 2012, ApJ, 747, 61
Young J. S., Devereux N. A., 1991, ApJ, 373, 414

This paper has been typeset from a TEX/LATEX file prepared by the author.